ARTICLE

Spatial Separation of Plasmonic Hot-Electron Generation and a Hydrodehalogenation Reaction Center Using a DNA Wire

Sergio Kogikoski Jr.,* Anushree Dutta, and Ilko Bald*

Read Online

ACCESS | Metrics & More | Article Recommendations | Supporting Information

ABSTRACT: Using hot charge carriers far from a plasmonic nanoparticle surface is very attractive for many applications in catalysis and nanomedicine and will lead to a better understanding of plasmon-induced processes, such as hot-charge-carrier- or heat-driven chemical reactions. Herein we show that DNA is able to transfer hot electrons generated by a silver nanoparticle over several nanometers to drive a chemical reaction in a molecule nonadsorbed on the surface. For this we use 8-bromo-adenosine introduced in different positions within a double-stranded DNA oligonucleotide. The DNA is also used to assemble the nanoparticles into nanoparticles ensembles enabling the use of surface-enhanced Raman scattering to track the decomposition reaction. To prove the DNA-mediated transfer, the probe molecule was insulated from the source of charge carriers, which hindered the reaction. The results indicate that DNA can be used to study the transfer of hot electrons and the mechanisms of advanced plasmonic catalysts.

KEYWORDS: plasmonics, DNA nanotechnology, hot electrons, charge transfer, SERS, superlattices
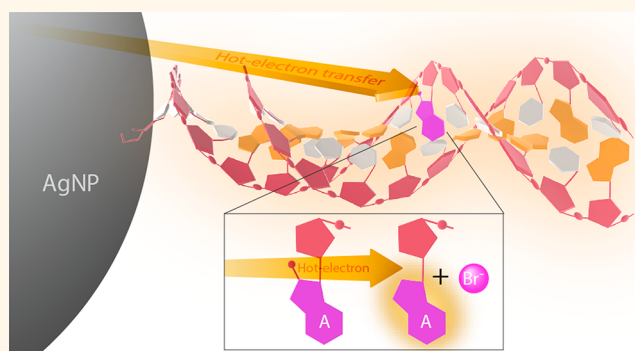
INTRODUCTION

One of the most interesting and promising uses of plasmonic nanoparticles is the possibility to induce chemical reactions at their interface giving rise to the emerging field of plasmon chemistry. The reactions are driven by different processes occurring at the interface between the plasmonic nanoparticle and the molecules, such as the generation of hot carriers and the thermalization of these carriers into heat. Even though it is very difficult to distinguish the contribution of the two mechanisms, both are suggested to affect the reaction pathways to some extent.[1,2] For both cases, there is the necessity of close contact of the reagent molecule with the nanoparticle surface, i.e., covalent bonding or adsorption, to activate it to further undergo the reaction.[3,4] This interaction can be problematic leading principally to the inactivation of the nanoparticle surface due to surface poisoning or undesired product generation, such as amorphous carbon.[5−8]

So far, many molecules have already been shown to react on the surface of illuminated plasmonic nanoparticles, like CO_2, H_2, 4-nitrothiophenol, and other organic molecules which were recently reviewed by Gellé et al.[9] The case of the dimerization of 4-nitrothiophenol is the most studied since the reaction can be directly tracked using surface-enhanced Raman spectroscopy (SERS), which can also be used to study the reaction

mechanism. Nevertheless, the mechanisms that trigger and direct the reaction pathways either by hot carriers or by heat are still under debate since the reaction involves many different steps, and at least 8 electrons to proceed.[2,10,11] Our group recently has shown that brominated nucleobases can undergo a plasmon induced reduction when adsorbed onto gold or silver nanoparticles, and that the reaction can be tracked using SERS.[12−14] The hot electrons generated on the nanoparticles are transferred to the brominated nucleobase which is followed by cleavage of the C−Br bond generating the nonbrominated base, in a procedure that only requires one electron and one proton via a dissociative electron attachment (DEA) mechanism.[15] Here we study this reaction with the brominated nucleobase incorporated in double-stranded DNA.

Transferring hot electrons generated in the plasmonic nanoparticles to a different material is a very interesting
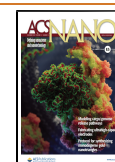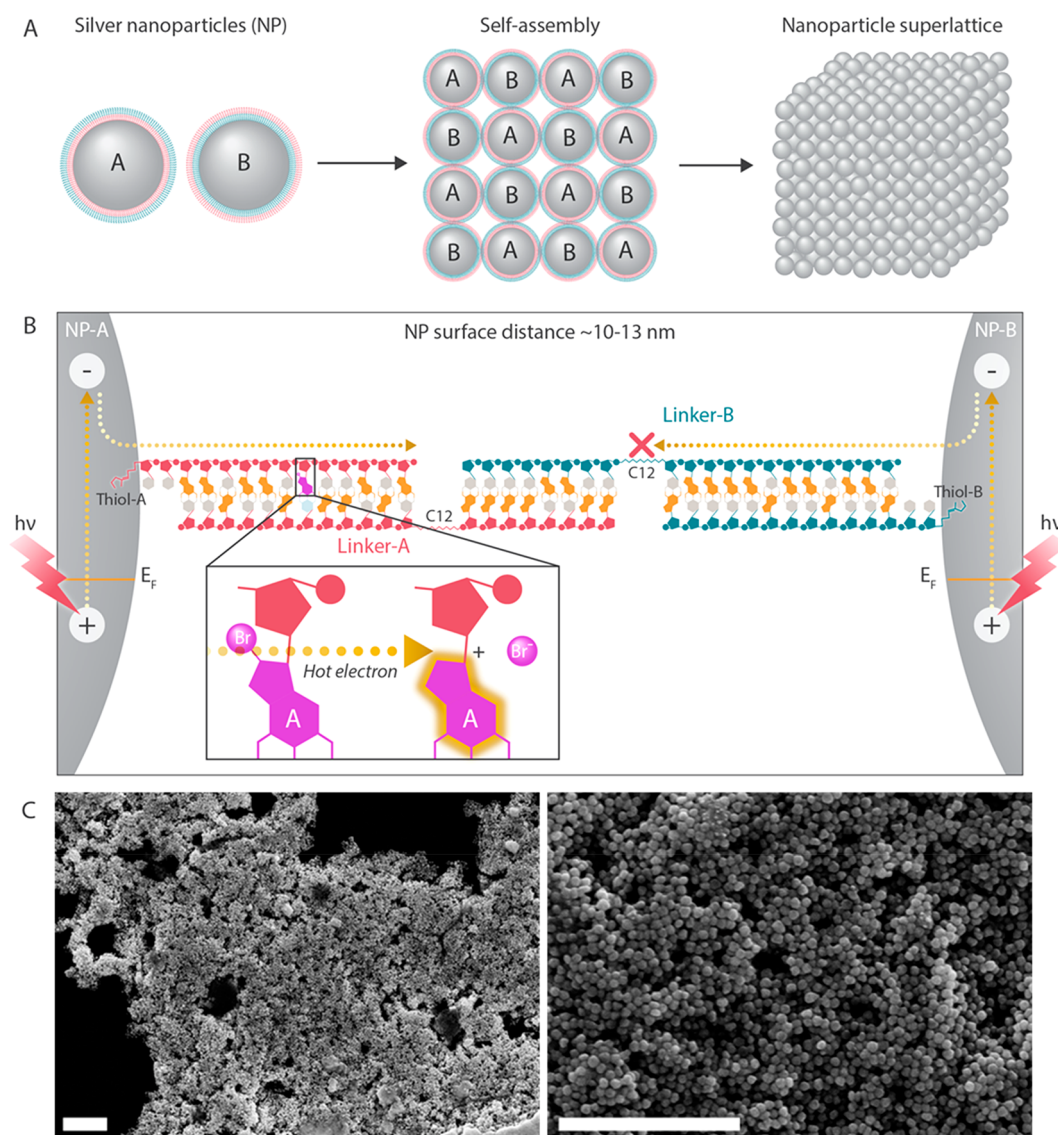
Figure 1. Schematic showing the AgNP superlattice ensembles. (A) AgNP modified with DNA sequences A and B, are mixed together and by base-pairing complementarity it can self-assembled in large nanoparticles superlattices. (B) DNA base-pairing between the sequences A and B brings the two nanoparticles together with a distance between 10 and 13 nm. The 8BrdA modification is inserted into sequence A, here shown in purple at position 7. Upon light irradiation, the nanoparticles generate a hot electron and hot hole pair. The hot electron can then be injected into the DNA double helix, enabling the hot electron reaction. All nanoparticles in the lattice can generate hot carriers, but due to the C_{12} chain each nanoparticle is insulated from the other, allowing precise control of the separation distance. (C) SEM images of the formed AgNP ensembles; the white scale bar represents 1 μm, which is similar in size to the laser spot size used to probe the reaction.

topic, principally because it can lead to a better understanding of plasmon-induced interfacial properties. Recently, Zhang et al.[16] showed that hot electrons can be transferred from Au nanoparticles to semiconductors and can go as far as 10 nm in semiconductors or 1 nm in metals, as well as being able to perform the dimerization reaction of 4-aminothiophenol very efficiently. In this case, the authors showed that the generated hot electrons are very quickly converted to heat in the metal, while in the semiconductor they can have a longer lifetime, enabling a long-range transmission. In contrast, Kim et al.[17] showed that hot electrons can be transferred by multistep hopping through an insulating layer of aliphatic chains self-assembled on Au nanoparticle surfaces over more than six carbons. Another interesting photocatalyst assembly was reported by Ma et al.[18] where the authors used DNA to self-assemble TiO_2 nanoparticles with CdS nanorods, enabling

electrons to be transferred from the TiO_2 to the CdS and facilitating CO_2 reduction. In this case, DNA is used as an electron-transfer mediator or a molecular-scale conductive wire, helping to promote better charge separation and increase the reaction yield. In this regard, we hypothesize that DNA can serve as an efficient mediator to conduct hot electrons generated from plasmonic nanoparticles and that these hot electrons will remain reactive to perform chemical reactions.

DNA is nowadays one of the most versatile biomolecules to obtain 2D and 3D nanostructures. Due to the very unique base pair arrangement, it is possible to create a wide variety of assemblies.[19−22] One important technique is DNA-based crystal engineering, where DNA is responsible for forming and maintaining the structure, while the nanoparticle is the rigid and directional entity, generating the so-called nanoparticle superlattices or programmable atom equivalents

(PAEs) ensembles. Crystal engineering with DNA has already enabled the fabrication of nanoparticles ensembles with a high degree of ordering with many different crystallographic orientations,[23] both using isotropic and anisotropic nanoparticles,[24,25] and even crystalline and epitaxial films were already obtained.[26−29] Due to the large efforts in crystallizing nanoparticles, many of the design and self-assembly rules governing the creation of superlattices are already well-described in the literature.[23,30] One of the most promising applications of DNA-based nanoparticle superlattices is the possibility of generating plasmonic materials with well-defined functionality.[25,26,31,32] However, in most of these cases DNA has limited functionality, and many of its properties regarding what the DNA chains are capable of is still limited. Recently, it was shown that the nanoparticles ensembles formed using DNA and 20 nm gold nanoparticles presented electrochemical conductivity and a very fast charge transfer (CT) rate which is mainly dependent on the DNA molecule.[33,34]

Herein we self-assembled 60 nm silver nanoparticle (AgNP) ensembles to probe hot-electron-induced reactions in single brominated nucleotides inserted into the DNA chains far from the nanoparticle surface. The nanoparticle ensemble design allowed us to provide electromagnetic enhancement enough to track the reduction of the brominated nucleotide by SERS in a single-point modification scale. Also due to the addressability offered by DNA it was possible to insert the modified base at very specific positions, allowing us to check the possibility of transferring hot electrons through DNA, which could enable further hot-electron-induced reactions to occur far from the nanoparticle surface. The obtained results showed that DNA is capable of transferring the hot electrons generated in the AgNPs to the reaction probe molecule far from the nanoparticle surface. It also indicates that the use of DNA-based superlattices provides a good platform to carry out hot-electron-driven reactions in a very controlled way. Herein we show that brominated nucleobases inserted into DNA can be decomposed by plasmonically generated hot electrons far from the nanoparticle surface, i.e., >5.5 nm.

RESULTS AND DISCUSSION

Design of the Nanoparticle−DNA Ensembles. The present study revolves around two central questions: (i) Is it possible to transfer hot carriers from AgNP through DNA? (ii) Is this hot carrier able to react with a specific molecule? A 3D superlattice is an ensemble of nanoparticles which is organized in a way that resembles an atomic crystal arrangement, i.e., there is a certain distance between the nanoparticle centers and there is a repetition unity in three dimensions. In this way, the nanoparticles are not simply aggregated but are arranged in a manner imparting a much more stable and uniform electromagnetic field than in a random aggregate. To accomplish this, we used DNA to act as the functional linking unit scaffolding the nanoparticles in place. In doing so, we select the DNA sequences with some considerations in mind: (i) The DNA sequences should be short enough to allow for the formation of plasmonic hot spots, enabling to track the reaction pathway using SERS. (ii) The hot carrier participation in the reaction should come from only one nanoparticle, so the reactant molecule should be insulated from the carriers coming from other nanoparticles. (iii) The DNA should only contain one modified base per sequence, in order to know the correct positioning of the base in relation to the nanoparticle surface.

Taking into consideration these points and also the existing rules to self-assemble the superlattices, we designed a system composed of 4 different DNA sequences, which are referred to as thiols A and B and linkers A and B. A model of the current system is illustrated in Figure 1. The two thiol sequences present a dithiolserinol group at the 3′ end to allow the easy modification of silver nanoparticles (SH groups at the end of the sequences), followed by a short flexible sequence composed of 5 cytosine (dC), which also interact with the nanoparticle surface, bringing the first base after it closer to the nanoparticle. After this there is a sequence containing 12 bases only composed of cytosine (dC) and guanine (dG), those 12 bases are complementary to 12 bases present at the linker sequences forming double helices. In the linker sequence there is a C_{12} aliphatic chain after the complementary sequence separating the first 12 bases from the next 8 bases, which stick to the complementary DNA present on the other sequence. The C_{12} aliphatic chain was chosen since it is long enough to hinder the charge transfer from the nanoparticles while at the same time imparting flexibility to the sequences toward proper assembly. In Figure 1, the 4 different DNA strands and the positions of modifications related to the nanoparticle surfaces are shown. The used sequences are given in Table 1.

Table 1. DNA Sequences Used in This Work

name	sequence ($5′ → 3′$)
thiol A	GCC CCG CCG CCG CCCCC−(SH)
thiol B	GCG CCG CGG CGG CCCCC−(SH)
thiol A1	GCC CCG CCG CC(8BrdA) CCCCC−(SH)
thiol A3	GCC CCG CCG (8BrdA)CG CCCCC−(SH)
thiol A7	GCC CC(8BrdA) CCG CCG CCCCC−(SH)
thiol A12	(8BrdA)CC CCG CCG CCG CCCCC−(SH)
linker A	CGG CGG CGG GGC−(C_{12})−CCG GCC CC
linker B	CCG CCG CGG CGC−(C_{12})−GG GGC CGG
linker A1	TGG CGG CGG GGC−(C_{12})−CCG GCC CC
linker A3	CGT CGG CGG GGC−(C_{12})−CCG GCC CC
linker A7	CGG CGG TGG GGC−(C_{12})−CCG GCC CC
linker A12	CGG CGG CGG GGT−(C_{12})−CCG GCC CC
linker AM	CGG CGG CGG GGC−(C_{12})−CCG G(8BrdA)C CC
linker BM	CCG CCG CGG CGC−(C_{12})−GG GTC CGG

The design chosen provides a distance between nanoparticle surfaces of around 10−13 nm, which can generate a strong enough plasmonic coupling to allow the detection of the single DNA base modifications by SERS, as can be observed in Figure 2B,C. The modified base 8-bromo-adenosine (8BrdA) was chosen as the reactive probe molecule, which is shown as a modified purple base in the Figure 1. Previous results from our group showed that the 8-bromo-adenine nucleobase is decomposed by hot-electron transfer from nanoparticles and that the signals from both the reactant and product present a very strong SERS signal, allowing us to track the reaction by Raman spectroscopy.[12,13] The chemical structures of 8BrdA and the products adenosine and a bromide anion are given in Figure 1.

Another advantage of 8BrdA is that it can easily be inserted into the oligomer during the synthesis without hindering the double helix formation later. In this way, 8BrdA is inserted into specific positions of the DNA sequence thiol A, and at the same time a complementary T was inserted into the linker sequences. 8BrdA was inserted into the positions 1, 3, 7, and 12 of the thiol A sequences, corresponding to approximately
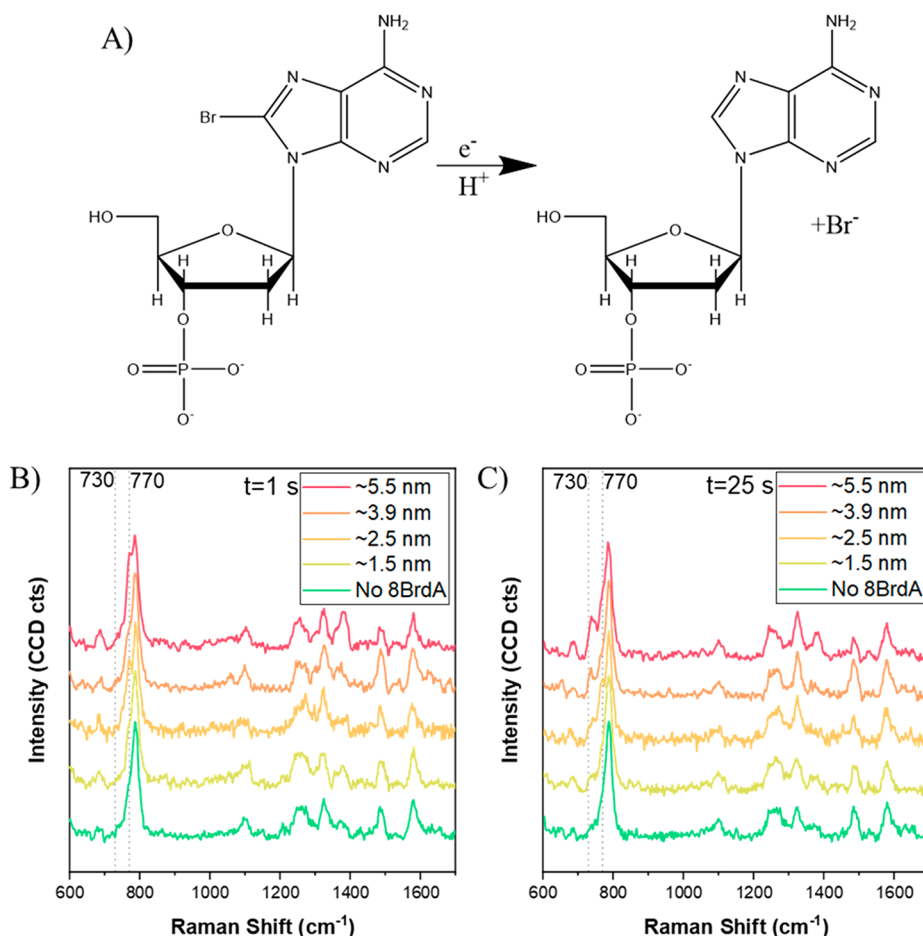
Figure 2. Hydrodehalogenation reaction tracked using SERS. (A) Due to the nanoparticle irradiation, hot electrons are ejected which can interact with 8BrdA cleaving the C−Br bond at the C-8 position, generating an adenosine base and a bromide anion. (B) SERS spectra recorded at t = 1 s, just after the irradiation is started for five different samples containing 8BrdA at different positions indicated by distance (nm) from the nanoparticle surface as mentioned in the legend. The samples containing 8BrdA present a peak or shoulder at the region around 770 cm^{-1}. (B) SERS spectrum collected after 25 s of irradiation. In the samples containing 8BrdA, the presence of a peak around 730 cm^{-1} corresponding to the adenosine ring-breathing vibration is clearly observed with no clear signature of the same in the control sample (green). The laser intensity for these spectra is 200 μW.

1.5, 2.5, 3.9, and 5.5 nm separation between the nanoparticle surface and the reactant molecule. A sample without 8BrdA is used as control for the test of the stability of DNA. SEM images (Figure 1C) confirm that the nanoparticles are self-assembled in a tightly packed configuration and that the ensemble is three-dimensional are larger than 1 μm in diameter, in such way that the Raman laser spot is completely probing the reaction in the nanoparticle ensemble and not the SiO$_2$ substrate. Small-angle X-ray scattering (SAXS) showed the formation of the nanoparticle ensemble, indicated by the diffraction pattern (Figure S1). The distance between nanoparticle surfaces obtained from SAXS is of about 13 nm, near the upper limit of the nominal distance shown before.

The choice of 8BrdA provides the possibility to detect single modifications by SERS based on its characteristic ring-breathing mode even when 8BrdA is surrounded by CG bases. Figure 2B shows the presence of the ring-breathing mode of 8BrdA in the region around 770 cm^{-1} in the SERS spectra, while the region around 730 cm^{-1} is clear of vibrational bands. After 25 s of irradiation (Figure 2C), the spectra show the presence of a very well-defined vibration at 730 cm^{-1} corresponding to the ring-breathing mode of adenosine, while the peak at 770 cm^{-1} is diminished allowing

us to track the decomposition of the 8BrdA and the appearance of adenosine over time. Additionally, we observe less intense vibrations related to the DNA backbone principally in the region between 1000 and 1600 cm^{-1} as seen in Figure 2B,C.[35] It is important to stress that the peaks corresponding to DNA backbone remain unaffected during the reaction and the reaction takes place specifically at the 8BrdA. That is to say, the rest of the DNA is not under the impact of the hot electrons for the laser power used.

Decomposition of 8BrdA in DNA. Since we could observe that after a certain time the 8BrdA is decomposed and that the adenosine is being formed, we then tracked the reaction for a longer period collecting SERS spectra throughout the reaction in order to study or comment on the reaction rate of hydrodehalogenation reaction under different experimental parameter. Figure 3A shows the time-dependent spectra between 0 and 70 s of irradiation, and it is possible to observe the instantaneous appearance of the adenosine peak at 734 cm^{-1} with decrease in peak intensity of 8BrdA at 765 cm^{-1} with time. We tracked the reaction over a period of 800 s, and the intensity map is shown in Figure 3B. The map in Figure 3B shows an intense vibration of 8BrdA in the beginning of the reaction that rapidly decreases with
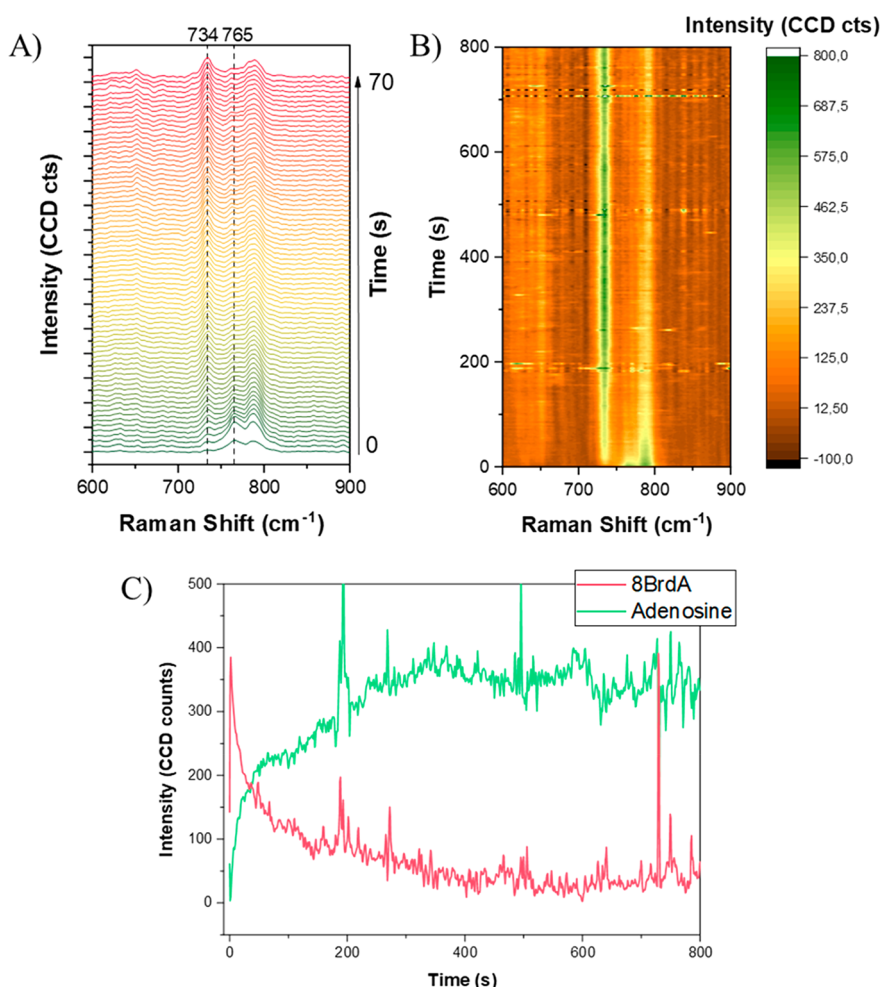
Figure 3. 8BrdA decomposition over time. (A) Time series SERS spectra of the sample with 8BrdA at ∼2.5 nm in the ring-breathing region (the two marked bands are related to the 8BrdA at 765 cm^{-1} and to adenosine at 734 cm^{-1}) over the period of 70 s, using a 1 s integration time. (B) Time series map for the sample with 8BrdA at ∼2.5 nm showing the progress of the reaction during 800 s. (C) Reaction time traces extracted from the time series shown in B, reflecting the kinetics of 8BrdA decay at 765 cm^{-1} and the formation of adenosine due to increase peak intensity at 734 cm^{-1}.

continuous increase of the adenosine peak over time. During the reaction we also observe the presence of flare emissions which are not associated with the reaction, but these were recently attributed to atomic dislocations of the metal atoms in the nanoparticles.[36]

It is possible to obtain the kinetics from the time traces for both the decomposition of 8BrdA and the generation of adenosine from all the collected spectra. The time trace data extracted from Figure 3B is shown in Figure 3C. The plot in Figure 3C shows that the 8BrdA vibration intensity decreases very rapidly and that the first 100 s of irradiation are sufficient to decrease the counts by around 300 s, after which the drop in peak intensity becomes slow until the irradiation is stopped. However, a concomitant rise in peak at 765 cm^{-1} corresponding to adenosine vibration can be observed with time. Recently, Liu et al.[37] proposed a very interesting mechanism for the plasmon-mediated hydrodehalogenation reaction of 8-bromo-adenine and the many reaction steps. We have also recently commented on the role of hole deactivation and the plasmonic substrate to fulfill the reaction cycle for both brominated purines.[14]

One of the most interesting properties of DNA is the possibility to transfer charges along the double helix. Such

property was observed by Jacqueline Barton in the 1990s by a series of photophysical studies of DNA intercalating molecules and base pair damage, and later it was also extensively studied by electrochemical methods.[38−42] Even with many different contributions, nowadays it is still a topic under intense debate principally regarding the flexibility of DNA[43] and also the possibility of the charge transfer to happen in the sugar backbone and not in the base pairs.[44] At the same time, it was also reported that DNA could be used to transfer hot electrons generated by Ag or AuNP and that the excess charges could quench a fluorophore or lead to intense DNA degradation, but in those cases, the nanoparticles were irradiated with high-intensity pulsed lasers.[45,46] Here in our case, we used a continuous wave laser to track the hot-electron-driven reaction showing that DNA is able to act as a conductive wire for hot-electron transfer and that the hot electrons are able to selectively break bonds in modified DNA bases.

Our understanding of the charge transfer mechanism is based on a three-step process.[47] The first step is the charge generation by the illuminated nanoparticles and the charge injection into the DNA chain after crossing an electron injection barrier; the second step is the actual charge transfer through DNA until it reaches the reaction point. The third step

Scheme 1. Schematic of the Control Experiment[a]
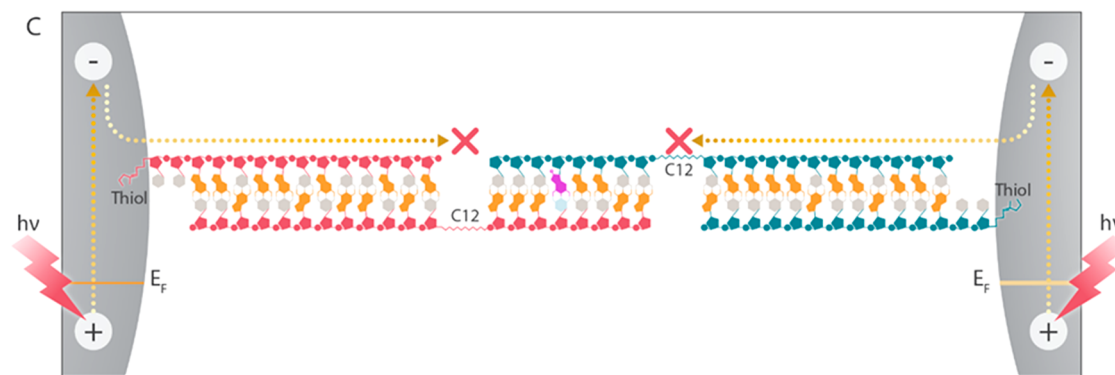
[a]In this case, 8BrdA (shown in purple) is included between the two C_{12} chains which hinder hot-electron passage from the nanoparticles, preventing the decomposition of the probe molecule.

is charge usage by an acceptor group, in our case 8BrdA. The charge transfer through DNA is very efficient and can achieve very high electron transfer rates (k_{ET}), from 10^2 s^{-1} measured by electrochemical methods[48−50] to 10^{10} s^{-1} measured by optical methods.[39] Those studies also measured the dependence of the rate on the distance, which was shown to be distance independent. According to the Marcus−Levich−Jortner correlation $k \propto e^{-\beta*r}$,[51] i.e., the rate would decrease exponentially depending on the distance r, β is the decaying constant. For DNA, the usual value for β is close to 0, meaning that the charge transfer is independent of the distance and that the energy loss due to the charge transfer is also very small, so the energy that the electron has when it is injected into DNA will remain constant without severe losses. In this way, we can rationalize that the highest energy loss will be associated with the injection into the DNA, and later the hot-electron energy will remain the same independent of the position of the modified nucleotide. From the three charge transfer steps, usually the charge injection is considered the rate-limiting step for the charge transfer, with an energy barrier which can vary between 0.2 and 0.4 eV.[47,52]

This energetics considerations helps us to rationalize how much energy the generated hot electron needs to proceed with the reaction. Previously, our group has shown by low-energy electron attachment experiments in the gas phase that the 8-bromoadenine is fragmented at three different energies of electron attachment, ∼0, 0.35, and ∼1 eV.[15] This experimental results indicates that the electron does not need to have high energy for such a dissociation reaction to proceed, since it is possible that even at ∼0 eV the C−Br bond is broken. Thus, the electron needs between 0.2 and 0.4 eV to overcome the first injection barrier, then be transferred and later react with 8BrdA. In the Supporting Information, a simplified schematic of such process is presented.

To further confirm and prove the charge transfer process, we modified the DNA sequence by incorporating the 8BrdA (purple base) in the stitch region in between two C_{12} chains (Scheme 1). As explained before, an aliphatic C_{12} chain should be long enough to fully hinder the conduction of electrons from the nanoparticles to the probing zone. The time series spectra and map of the samples corresponding to insulated 8BrdA is shown in Figure 4A,B. Interestingly, it is possible to observe an intense 8BrdA peak at 765 cm^{-1}, which is still fully visible after 100 s of irradiation, while the peak for the adenosine appears only after 50 s of irradiation, but with very

low peak intensity. This is in contrast to when compared with the data shown in Figure 3A where the adenosine peak appears right after the irradiation showing a strong intensity peak.

From the map shown in Figure 4B, the kinetic time traces can be extracted for both 8BrdA decomposition and adenosine formation, which are then compared to the case where the 8BrdA is connected to the DNA sequence exposing it to the source of the hot electron. In this case, we compare with the sample where the 8BrdA is the farthest away from the nanoparticle surface (∼5.5 nm). This comparison is given in Figure 4C,D. The data comparison shows that the C_{12} chains do hinder the hot-electron passage and that the 8BrdA reaction does not proceed. The slight decrease in 8BrdA intensity over a long time and the increase of the adenosine vibration are probably not due to a DEA reaction but possibly are due to the plasmonically generated heat that can also induce reactions leading to molecular decomposition. The distinction between the hot-electron- and the heat-driven reactions is usually very difficult since both processes are happening at the same time and since both can take the same reaction pathway. Herein we show that the use of a DNA wire can help to disentangle both contributions.

So far, we showed that DNA can be used to control self-assembly of nanoparticles which are useful for SERS analysis, that the hot electron is being transferred through DNA far away from the nanoparticle surface, and that it can be used to drive reactions within DNA. In the next section, the kinetics of the hot-electron-driven reaction will be discussed, focusing on the decomposition process of 8BrdA and the relationship between the experimentally determined kinetic constant to its position in the DNA sequence and the contribution of the laser power to the reaction.

Probe Molecule Position and Laser Power Dependence. To assess the reaction under different experimental reaction condition and parameters, we differ the probe molecular position with respect to the surface and monitor their reaction kinetics under different laser power. As discussed before, due to the many possible steps which could involve the formation of adenosine we will focus our discussion on the decomposition of 8BrdA. We have modeled the reaction of 8-bromoadenine with hot electrons before by a DEA mechanism.[15] In this mechanism, an electron is captured at a specific energy to form a transient negative ion (TNI), which can dissociate very quickly, resulting in the adenine nucleobase, the structure of the molecules we are probing here were shown
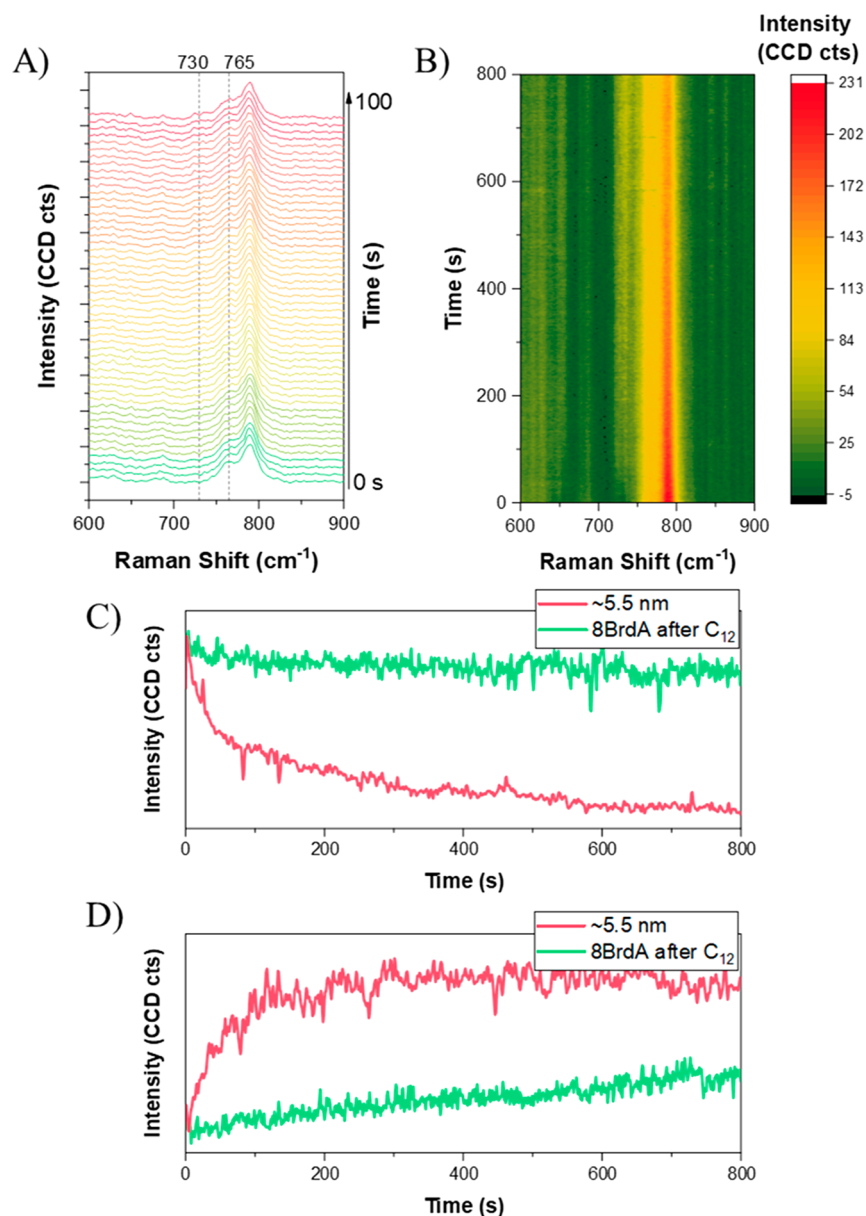
Figure 4. Control experiment of the insulated 8BrdA. (A) Timed spectra in the ring-breathing vibration mode of the sample with 8BrdA located between the C_{12} chain. The two marked bands are related to the 8BrdA at 765 cm^{-1} and to adenosine at 730 cm^{-1} over the period of 100 s, using a 1 s integration time. **(B)** Time series SERS map of the sample with the 8BrdA after the C_{12} chain, showing the progress of the 8BrdA decomposition reaction upon laser irradiation. **(C and D)** Comparison of the experimental reaction time traces for the region of 8BrdA **(C)** and adenosine **(D)** vibrations. The control experiment where 8BrdA is insulated is compared to the time traces for the sample with 8BrdA at ~5.5 nm (the farthest possible position of 8BrdA regarding the nanoparticle surface). The conditions for the spectra acquisition are as follows: 1 s integration time, laser power of 500 μW in the focal plane.

in Figure 2A. The fitting procedure used to obtain the kinetics constants is given in the Supporting Information. Herein we used a second-order fractal kinetics equation to fit the obtained kinetics time traces.

The consideration about the fractal-like system arises from the nanoparticle organization in the nanoscale and the intrinsic inhomogeneity of the SPR excitation in the system. On a nonfractal regime, the reaction rate constant k would be the same all around the nanoparticle surface. However, the close proximity between the nanoparticles creates the so-called hot spots, which are regions that can promote a faster reaction rate, but since this is not homogeneously spread over the nanoparticle surface but constrained in some regions, it can

create regions with different k that vary over time. After the initial consumption of the probe molecules located at the most intense hot spots (k_1), the rest of the molecules on the nanoparticle surface will react but slower compared to the hot spot reaction $(k_2, k_3, k_4, ..., k_n)$, creating a gradient of rate constants in the system, and the relative contribution of each k is dependent on the time such as shown by Schürmann and Bald.[12] The reaction kinetics in our case follows a second-order fractal kinetics rate law:

$$[8BrdA] = \frac{[8BrdA]_0 \cdot (1 - h)}{(1 - h) + [8BrdA]_0 \cdot k_{2F} \cdot t^{1-h}} \quad (1)$$
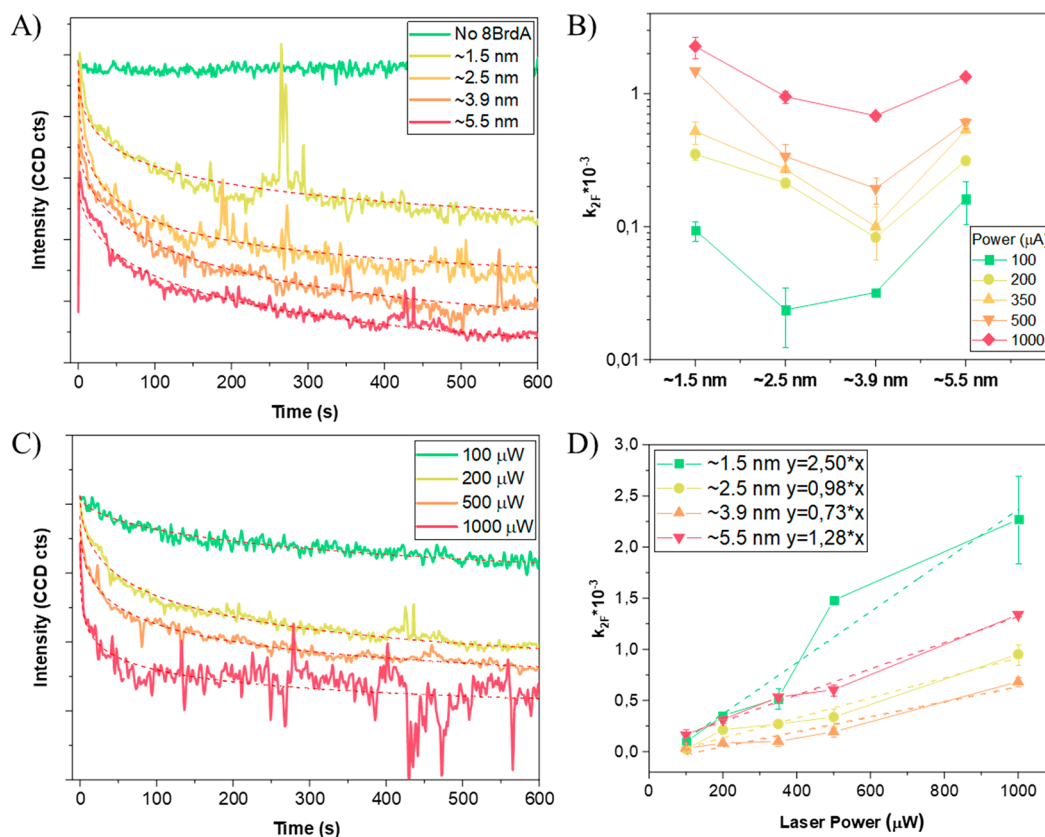
Figure 5. Effect of the base placement and laser power on the 8BrdA decomposition reaction. (A) Comparison of the experimental reaction traces for different samples containing 8BrdA. The data are offset for better visualization; the data were extracted from the experiment obtained using a laser power of 200 μW. The red traced curves show the fit of the data using the second-order fractal kinetics (eq 1). (B) Comparison between the k_{2F} obtained from the fits in A and the position of 8BrdA in the DNA for different laser powers. (C) Comparison of the experimental kinetic traces using different laser powers. The red traced curves show the fit of the data using the second-order fractal kinetics (eq 1). The data shown here are related to the sample containing 8BrdA at ~5.5 nm from the AgNP surface. (D) Experimental relationship between k_{2F} with the laser power for the 4 samples containing the 8BrdA at different positions. The red traces show the linear fit of the points for each one of the samples, and the linear equation describing each data set is given in the figure legend.

where [8BrdA] is the intensity of the 8BrdA peak in the Raman spectra, [8BrdA]$_0$ is the initial intensity of the 8BrdA peak in the Raman spectra, k_{2F} is the second-order fractal rate constant, t is the time, and h is the fractal dimension term. This equation can fit the data directly extracted from the Raman spectra, and from the fit the second-order fractal rate constant is obtained. The derivation of this equation is given in the Supporting Information. The use of a simplified second-order fractal reaction equation allows us to fit all the data, and according to our energy considerations (described previously), it allows us to approximately calculate the number of hot electrons being generated over time: At 1 mW of laser excitation, ~60 hot electrons per second should be generated, and there is no excess of hot electrons participating in the reaction. Due to the charge injection process and DNA CT, it is plausible to say that only one electron is actively participating in the reaction on each DNA chain; thus, the concentrations of 8BrdA and hot electrons are very close.

The first point of our discussion here is the position of the probe in the DNA chain. The data showing the extracted time traces for the samples with different 8BrdA positions are given in Figure 5A. For the control where no 8BrdA is present in the DNA chain, we obtain a straight line without any decrease in intensity (at the ~770 cm^{-1} region of the spectra), indicating that DNA is stable under the experimental conditions

employed. Upon the inclusion of the 8BrdA in the DNA double helix, it is now possible to observe and track the decomposition of the probe molecule. The data in Figure 5A shows that the decomposition of 8BrdA takes place for all the cases when 8BrdA is included in the DNA.

From the kinetic analysis we obtain the value of the second-order fractal kinetics rate constant k_{2F}. In Figure 5B, it is shown how the k_{2F} varies depending on the probe position on the DNA chain and hence with the distance to the nanoparticle surface. This is shown for different laser powers, which will be discussed later. The distance dependence of k_{2F} follows a U-shaped profile, i.e., the rate constant is high when the probe is the closest to the surface (about 1.5 nm), then decreases in the middle position (2.5 and 3.9 nm), and is again very high when furthest away from the surface (around 5.5 nm). As discussed before, the conduction through DNA is still a topic under debate, but we can include some considerations regarding the topic here.

One very important aspect of our system is the DNA sequence used. The sequences used here are very rich in CG base pairs which have a very interesting conduction aspect. One of the most accepted mechanisms of DNA conduction assumes that the conduction occurs by a mixed process involving both tunneling and multistep hopping.[51,53,54] Giese et al.[51,55] observed that hopping through the CG base pairs is

very much favored due to the lower redox potential of the G nucleobase. The possibility of the AT pair to conduct holes by hopping was later tested by the same group. More recently, Xiang et al.[56] showed that having an ordered array of CG base pairs can enhance DNA conductivity a bit due to the HOMOs of the stacked Gs being delocalized over several G bases, as in our case where some G bases are stacked helping the electron transfer. The most interesting property of the hopping-like mechanism is that it is distance independent, i.e., the charge carrier can be transferred through long DNA sequences without losing its energy.[42] In our results, we can observe that even with the probe ∼5.5 nm far from the nanoparticle surface the reaction is still happening at a similar rate as when it is the closest at ∼1.5 nm. Another aspect of DNA charge transfer was studied recently by Kékedy-Nagy and Ferapontova,[50] who showed a very interesting asymmetry of the DNA-mediated charge transfer toward the reduction of methylene blue and found that charge transfer in the forward direction is faster than in the backward direction, an indication that DNA can also be used to avoid charge recombination, increasing the reaction rate for the generation of the products since the electrons can live longer within the DNA double helix.

The U-shape profile of the observed k_{2F} can be explained by two possibilities. Recently, Li and Han demonstrated by simulations that the stacking of the DNA bases can alter the long-range charge transfer through DNA.[57] The authors suggest that due to the stacking of the orbitals, it is possible to form a potential well with depth of 0.1−0.3 eV *in vacuo*, which stabilizes the base pairs in the middle of the sequence while at the same time leads to a lower stabilization of the base pairs in the edge of the sequence, which in turn could enhance the reactivity of such bases toward an external agent, such as the nanoparticle-generated hot electrons.[58] The present data can suggests that 8BrdA located at the edges is subject to a lower stabilization due to the incomplete stacking by the π-orbital clouds of the DNA double helix, making it more prone to the reaction with hot electrons. At the same time, the probe molecules located in the middle of the sequence are much more stabilized by the other bases around it, making it harder to decompose via the hot electrons thereby decreasing the reaction rate. Another possible explanation is related to the DNA charge transfer mechanism, since both tunneling and hopping are part of the charge transfer process. The reactive group is an 8BrdA−dT pair, which creates an energetic barrier in the long dCdG chain. The charge can be either inserted into the 8BrdA (by hopping) and induce the decomposition reaction, or it can tunnel through the barrier (8BrdA−dT bp), lose energy, and then be unavailable for the reaction due to the energy loss. The fact that a charge can tunnel through single AT barriers is well described in literature[55,56,59] and can also be a reason for the lower reaction rate observed for the bases in the middle of the chain. A possible scheme of this process is given in the Figure S3. The data presented in Figure 5B also shows the dependence of the reaction rate on the laser power used for the irradiation, which will be discussed next.

The laser power affects a plasmon-induced reaction in two different ways: On the one hand, a higher laser power results in generation of more hot electrons increasing the reaction rate by increasing the number of reactants hot electrons. On the other hand, it can be converted to heat due to the thermalization of the hot carriers, and the reaction is faster due to the thermal contribution.[1,4,60] Disentangling both contributions is very hard principally because both processes happen at the same time (at least in the time scales discussed here in this work). The time traces for the sample containing 8BrdA far from the AgNP surface, i.e., ∼5.5 nm, at different laser powers is given in Figure 5C. The decomposition rate of 8BrdA is directly proportional to the increase in laser power, i.e., at higher laser powers the reaction proceeds faster compared to low laser powers. At the same time, we observe that at high laser powers (1000 μW) the reaction reaches a plateau in less than 100 s and that the continued irradiation leads to different processes observed by the very intense noise signal after 300 s. All the curves at different laser power were fitted using the second-order fractal integrated rate law, and the obtained k_{2F} values at different laser power is given in Figure 5D. The data in Figure 5B,D are the same, but the different representations give us hints on different processes.

The data in Figure 5D suggests that the reaction rate increases linearly with the laser power, especially for the samples with 8BrdA at ∼2.5, ∼3.9, and ∼5.5 nm. The average value for the slope of the linear fit for these samples is 0.94, an indication that increasing the laser power directly increases the reaction rate by the same order of increase, while for the sample with 8BrdA very close to the AgNP surface (∼1.5 nm), the slope of the linear fit is 2.28. This is an indication that the reaction with slope closer to 1 represents a hot-electron-triggered reaction, while a higher slope value indicates that plasmonically generated heat is also contributing. Baffou and Quidant[61,62] showed that the heat dissipation for spherical nanoparticles under CW irradiation follows a $1/r$ distribution, i.e., the temperature decreases with increasing distance from the NP surface and the influence of thermal effects gets less as we can observe in Figure 5B,D. In conclusion, the high-rate constant observed for the sample with 8BrdA closer to the NP surface is not only due to a limited nucleotide stabilization at the beginning of the sequence but also due to some contribution of thermal energy.

We can observe the lowest rate for the sample with 8BrdA at ∼2.5 nm at a laser power of 100 μW, but increasing the laser power to 200 μW increases its rate more than that of the probe at 3.9 nm, making this sample now the slowest and keeping this pattern throughout the experiment. This shift is possibly due to the heat generated by the particle spreading further from the particle surface; however, it does not increase as fast as when the probe molecule is at ∼1.5 nm. At ∼3.9 nm, the reaction is not very much influenced by the heat generated by the particles, and the reaction is slower than the other positions, an indication that DNA provides a stabilized structure. The hot electrons are probably distributed through the chain which decreases the reactivity of the 8BrdA. Finally, when 8BrdA is very far from the nanoparticle surface it is only influenced by the hot-electron transfer and since it is at the end of the chain it does not have the full stabilization of DNA, making its reaction rate higher compared to the cases when the probe is in the middle of the chain but lower than the closest one since it is not subject to the extra energy input coming from the heated surface.

CONCLUSIONS

To conclude, herein we showcase the use of self-assembled nanoparticle ensembles for plasmon-induced reactions, and we demonstrate that DNA can be used to transfer hot electrons far from the nanoparticle surface. DNA allows us to build nanoparticle lattices with a very short interparticle spacing, and it also provides a suitable scaffold for controlled placement

of modifications. We used 8BrdA, known for its simple decomposition reaction pathway compared to other molecules, requiring only one electron and one proton for the reaction. The hydrodehalogenation reaction of 8BrdA at different positions followed a second-order fractal kinetics rate law with k_{2F} dependent on the position of the probe molecule in the DNA sequence and also on the laser power employed for irradiation. More than that, we show that by the correct placement of the probe molecule it is possible to control the hot-electron-driven pathway over the thermal pathway, principally due to hot-electron transfer through DNA.

The results shown here have many possibilities for plasmon-induced chemical reactions. So far, the reactions were confined to the surface of the plasmonic nanoparticle, while we show that this could occur further away from the nanoparticle surface using DNA as charge-conducting wire. Further understanding of the DNA−nanoparticle interaction at the interface and charge injection into DNA needs to be gained in future experiments. The possibility of transferring electrons from the DNA to molecules which are interacting with but are not covalently bound to DNA also needs to be explored in further studies. Optimizing the charge extraction process to carry out reactions that require more than one hot carrier also needs further attention. In the future, we hope that the study presented here serves as a basis to better understand plasmon-induced reactions which do not require direct contact with the nanoparticle surface.

EXPERIMENTAL SECTION

Materials. All chemicals were of the highest purity available and were used without further purification. Sodium citrate, TAE buffer 10×, sodium dodecyl sulfate (SDS), HCl, NaOH, and NaCl were obtained from Sigma-Aldrich. Silver nanoparticles with diameter of 60 nm stabilized by sodium citrate were obtained from Nanocomposix. The DNA sequences were all obtained from Metabion GmbH, and all the sequences were purified by HPLC and confirmed with mass spectrometry. Water was purified by a Milli-Q system.

Nanoparticle Modification and Superlattice Self-Assembly. To modify the AgNP with the thiolated DNA sequences, we adapted the low pH method protocol. In this procedure, the dispersion of nanoparticles and DNA are submitted to a lower pH by the addition of citric acid at pH 3.[63] For 1 mL of 60 nm AgNP, 2% SDS was added to a concentration of 0.02% and shaken for 20 min at 37 °C. Then an 8000-fold excess of thiolated DNA was added, i.e., around 4 μL of a 100 μM DNA-SH solution, and was left shaking for 20 min to fully interact with the AgNP. After 20 min, pH of the solution was changed to 3 by the addition of 500 mmol L^{-1} of citric acid, i.e., around 20−40 μL is sufficient for the change. After 10 min more shaking at 37 °C, the pH of the solution is restored to around 7 by the addition of the same volume of 10× TAE buffer. Using these conditions, the concentration of Na$^+$ in solution is around 100−200 mmol L^{-1}. This step adds the thiolated DNA to the nanoparticle surface in a very high yield.

Next to the modified nanoparticle solution, 16 000× excess of the linker sequence is added in solution, and the mixture is heated to 75 °C for 15 min while shaking. This temperature promotes the full melting of the DNA oligomers. After this the AgNP solution is cooled off by 5 °C every 10 min until a temperature of 30 °C is reached which is then left for shaking at this temperature overnight. Next the nanoparticles are washed by centrifugation 5 times to remove any aggregate and nonbound DNA present in the solution. After every wash, the supernatant is removed, and the volume is made up with 50 mmol L^{-1} NaCl with 0.02% SDS. After every wash, the solution is sonicated in a bath sonicator for 1 min to break any nanoparticle aggregates. At the end the nanoparticle concentration is quantified by UV−vis spectrometry.

From the freshly modified nanoparticles the superlattice is assembled by mixing the nanoparticles modified with the sequence A and the ones modified with the sequence B in equimolar amounts. More NaCl is added to the solution to reach the concentration between 100 and 150 mmol L^{-1} of Na$^+$. The mixtures are then inserted into a thermocycler that is heated up to 50 °C for 15 min and is later cooled down to 20 °C over the course of 24 h. If the self-assembly proceeds correctly, then the formation of precipitates is observed; otherwise, the solution will keep its yellow color if the ensemble is not formed.

Raman Spectra Acquisition and Data analysis. SERS spectra have been recorded using a confocal Raman microscope (WITec 300α) equipped with an upright optical microscope. For Raman excitation, laser light at λ = 633 nm was used that was coupled into a single-mode optical fiber and focused through a 50× objective (Olympus MPlanFL N, NA = 0.75) to a spot size of about 1000 nm. The laser power was varied (100, 200, 500, and 1000 μW) at the focal plane, and the integration time was 1 s. The kinetics were followed between 5 to 15 min for each sample, i.e., each curve is based on 300−900 different spectra. Each sample was measured at least 3 times, and the results shown here are the average of all the different Raman measurements, i.e., all the spectra collected were averaged over time, and the time traces are extracted directly from the average data.

ASSOCIATED CONTENT

ⓈI Supporting Information

The Supporting Information is available free of charge at https://pubs.acs.org/doi/10.1021/acsnano.1c09176.

> SAXS results and discussion, discussion on the energetic analysis of the reaction pathway, kinetics modeling used in the fittings, estimation of the number of hot electrons generated over time and its relation to the energetics of the dehalogenation reaction (PDF)

AUTHOR INFORMATION

Corresponding Authors

Sergio Kogikoski Jr. − *Institute of Chemistry, Physical Chemistry, University of Potsdam, 14476 Potsdam, Germany; Department of Analytical Chemistry, Institute of Chemistry, State University of Campinas (UNICAMP), 13083-970 Campinas, São Paulo, Brazil;* Phone: +49 331-977-6114; Email: kogikoskijunior@uni-potsdam.de

Ilko Bald − *Institute of Chemistry, Physical Chemistry, University of Potsdam, 14476 Potsdam, Germany;* ⓞ orcid.org/0000-0002-6683-5065; Phone: +49 331-977-5238; Email: bald@uni-potsdam.de

Author

Anushree Dutta − *Institute of Chemistry, Physical Chemistry, University of Potsdam, 14476 Potsdam, Germany;* ⓞ orcid.org/0000-0001-5862-3233

Complete contact information is available at:
https://pubs.acs.org/10.1021/acsnano.1c09176

Author Contributions

S.K. and I.B. conceived the study. S.K. prepared all the samples, characterized them, and measured the decomposition reaction. S.K., A.D., and I.B. analyzed and discussed the data. All authors contributed to the manuscript writing.

Notes

A preprint of the manuscript was published online: Kogikoski, S., Jr.; Duttta, A.; Bald, I. Spatial Separation of Plasmonic Hot-ElectronGeneration and a Hydrodehalogenation Reaction Center Using a DNA Wire. *ChemRxiv*, March 1, **2020**, ver.

2.DOI: 10.26434/chemrxiv.14114306.v2 (accessed on November 17, 2021).

The authors declare no competing financial interest.

REFERENCES

(1) Jain, P. K. Taking the Heat off of Plasmonic Chemistry. *J. Phys. Chem. C* **2019**, *123*, 24347−24351.

(2) Koopman, W.; Sarhan, R. M.; Stete, F.; Schmitt, C. N. Z.; Bargheer, M. Decoding the Kinetic Limitations of Plasmon Catalysis: The Case of 4-Nitrothiophenol Dimerization. *Nanoscale* **2020**, *12*, 24411−24418.

(3) Mukherjee, S.; Libisch, F.; Large, N.; Neumann, O.; Brown, L. V.; Cheng, J.; Lassiter, J. B.; Carter, E. A.; Nordlander, P.; Halas, N. J. Hot Electrons Do the Impossible: Plasmon-Induced Dissociation of H2 on Au. *Nano Lett.* **2013**, *13* (1), 240−247.

(4) Miliutina, E.; Guselnikova, O.; Soldatova, N. S.; Bainova, P.; Elashnikov, R.; Fitl, P.; Kurten, T.; Yusubov, M. S.; Švorčík, V.; Valiev, R. R.; Chehimi, M. M.; Lyutakov, O.; Postnikov, P. S. Can Plasmon Change Reaction Path? Decomposition of Unsymmetrical Iodonium Salts as an Organic Probe. *J. Phys. Chem. Lett.* **2020**, *11* (14), 5770−5776.

(5) Novello, P.; Varanasi, C. V.; Liu, J. Effects of Light on Catalytic Activities and Lifetime of Plasmonic Au Catalysts in the CO Oxidation Reaction. *ACS Catal.* **2019**, *9* (1), 578−586.

(6) Liu, L.; Wang, Y.; Fu, W. Highly Selective Detection of Sulfide through Poisoning Silver Nanoparticle Catalysts. *Sens. Actuators, B* **2017**, *247*, 414−420.

(7) Szczerbiński, J.; Gyr, L.; Kaeslin, J.; Zenobi, R. Plasmon-Driven Photocatalysis Leads to Products Known from E-Beam and X-Ray-Induced Surface Chemistry. *Nano Lett.* **2018**, *18* (11), 6740−6749.

(8) Heck, C.; Kanehira, Y.; Kneipp, J.; Bald, I. Amorphous Carbon Generation as a Photocatalytic Reaction on DNA-Assembled Gold and Silver Nanostructures. *Molecules* **2019**, *24* (12), 2324.

(9) Gellé, A.; Jin, T.; De La Garza, L.; Price, G. D.; Besteiro, L. V.; Moores, A. Applications of Plasmon-Enhanced Nanocatalysis to Organic Transformations. *Chem. Rev.* **2020**, *120* (2), 986−1041.

(10) Choi, H. K.; Park, W. H.; Park, C. G.; Shin, H. H.; Lee, K. S.; Kim, Z. H. Metal-Catalyzed Chemical Reaction of Single Molecules Directly Probed by Vibrational Spectroscopy. *J. Am. Chem. Soc.* **2016**, *138* (13), 4673−4684.

(11) Schürmann, R.; Ebel, K.; Nicolas, C.; Milosavljević, A. R.; Bald, I. Role of Valence Band States and Plasmonic Enhancement in Electron-Transfer-Induced Transformation of Nitrothiophenol. *J. Phys. Chem. Lett.* **2019**, *10* (11), 3153−3158.

(12) Schürmann, R.; Bald, I. Real-Time Monitoring of Plasmon Induced Dissociative Electron Transfer to the Potential DNA Radiosensitizer 8-Bromoadenine. *Nanoscale* **2017**, *9* (5), 1951−1955.

(13) Dutta, A.; Schürmann, R.; Bald, I. Plasmon Mediated Decomposition of Brominated Nucleobases on Silver Nanoparticles − A Surface Enhanced Raman Scattering (SERS) Study. *Eur. Phys. J. D* **2020**, *74* (1), 19.

(14) Dutta, A.; Schürmann, R.; Kogikoski, S., Jr.; Mueller, N. S.; Reich, S.; Bald, I. Kinetics and Mechanism of Plasmon Driven Dehalogenation Reaction of Brominated Purine Nucleobases on Ag and Au. *ACS Catal.* **2021**, *11* (13), 8370−8381.

(15) Schürmann, R.; Tanzer, K.; Dąbkowska, I.; Denifl, S.; Bald, I. Stability of the Parent Anion of the Potential Radiosensitizer 8-Bromoadenine Formed by Low-Energy (<3 EV) Electron Attachment. *J. Phys. Chem. B* **2017**, *121* (23), 5730−5734.

(16) Zhang, H.; Wei, J.; Zhang, X. G.; Zhang, Y. J.; Radjenovica, P. M.; Wu, D. Y.; Pan, F.; Tian, Z. Q.; Li, J. F. Plasmon-Induced Interfacial Hot-Electron Transfer Directly Probed by Raman Spectroscopy. *Chem.* **2020**, *6* (3), 689−702.

(17) Kim, Y.; Wilson, A. J.; Jain, P. K. The Nature of Plasmonically Assisted Hot-Electron Transfer in a Donor-Bridge-Acceptor Complex. *ACS Catal.* **2017**, *7* (7), 4360−4365.

(18) Ma, K.; Yehezkeli, O.; He, L.; Cha, J. N. DNA for Assembly and Charge Transport Photocatalytic Reduction of CO2. *Adv. Sustain. Syst.* **2018**, *2* (4), 1700156.

(19) Laramy, C. R.; O'Brien, M. N.; Mirkin, C. A. Crystal Engineering with DNA. *Nat. Rev. Mater.* **2019**, *4*, 201−224.

(20) Tapio, K.; Bald, I. The Potential of DNA Origami to Build Multifunctional Materials. *Multifunct. Mater.* **2020**, *3* (3), 032001.

(21) Kogikoski, S.; Paschoalino, W. J.; Kubota, L. T. Supramolecular DNA Origami Nanostructures for Use in Bioanalytical Applications. *TrAC, Trends Anal. Chem.* **2018**, *108*, 88−97.

(22) Seeman, N. C.; Sleiman, H. F. DNA Nanotechnology. *Nat. Rev. Mater.* **2018**, *3*, 17068.

(23) Macfarlane, R. J.; Lee, B.; Jones, M. R.; Harris, N.; Schatz, G. C.; Mirkin, C. A. Nanoparticle Superlattice Engineering with DNA. *Science* **2011**, *334* (6053), 204−208.

(24) O'Brien, M. N.; Jones, M. R.; Lee, B.; Mirkin, C. A. Anisotropic Nanoparticle Complementarity in DNA-Mediated Co-Crystallization. *Nat. Mater.* **2015**, *14* (8), 833−839.

(25) Sun, L.; Lin, H.; Park, D. J.; Bourgeois, M. R.; Ross, M. B.; Ku, J. C.; Schatz, G. C.; Mirkin, C. A. Polarization-Dependent Optical Response in Anisotropic Nanoparticle-DNA Superlattices. *Nano Lett.* **2017**, *17* (4), 2313−2318.

(26) Ross, M. B.; Ku, J. C.; Blaber, M. G.; Mirkin, C. A.; Schatz, G. C. Defect Tolerance and the Effect of Structural Inhomogeneity in Plasmonic DNA-Nanoparticle Superlattices. *Proc. Natl. Acad. Sci. U. S. A.* **2015**, *112* (33), 10292−10297.

(27) Ross, M. B.; Bourgeois, M. R.; Mirkin, C. A.; Schatz, G. C. Magneto-Optical Response of Cobalt Interacting with Plasmonic Nanoparticle Superlattices. *J. Phys. Chem. Lett.* **2016**, *7* (22), 4732−4738.

(28) Gabrys, P. A.; Seo, S. E.; Wang, M. X.; Oh, E.; Macfarlane, R. J.; Mirkin, C. A. Lattice Mismatch in Crystalline Nanoparticle Thin Films. *Nano Lett.* **2018**, *18* (1), 579−585.

(29) Senesi, A. J.; Eichelsdoerfer, D. J.; Macfarlane, R. J.; Jones, M. R.; Auyeung, E.; Lee, B.; Mirkin, C. A. Stepwise Evolution of DNA-Programmable Nanoparticle Superlattices. *Angew. Chem., Int. Ed.* **2013**, *52* (26), 6624−6628.

(30) Macfarlane, R. J.; O'Brien, M. N.; Petrosko, S. H.; Mirkin, C. A. Nucleic Acid-Modified Nanostructures as Programmable Atom Equivalents: Forging a New "Table of Elements. *Angew. Chem., Int. Ed.* **2013**, *52* (22), 5688−5698.

(31) Ross, M. B.; Ku, J. C.; Lee, B.; Mirkin, C. A.; Schatz, G. C. Plasmonic Metallurgy Enabled by DNA. *Adv. Mater.* **2016**, *28* (14), 2790−2794.

(32) Young, K. L.; Ross, M. B.; Blaber, M. G.; Rycenga, M.; Jones, M. R.; Zhang, C.; Senesi, A. J.; Lee, B.; Schatz, G. C.; Mirkin, C. A. Using DNA to Design Plasmonic Metamaterials with Tunable Optical Properties. *Adv. Mater.* **2014**, *26* (4), 653−659.

(33) Kogikoski, S.; Kubota, L. T. Electrochemical Behavior of Self-Assembled DNA−Gold Nanoparticle Lattice Films. *Electrochem. Commun.* **2018**, *90*, 51−55.

(34) Kogikoski, S.; Kubota, L. T. Electron Transfer in Superlattice Films Based on Self-Assembled DNA-Gold Nanoparticle. *Electrochim. Acta* **2019**, *318*, 931−936.

(35) Guerrini, L.; Krpetić, Ž.; Van Lierop, D.; Alvarez-Puebla, R. A.; Graham, D. Direct Surface-Enhanced Raman Scattering Analysis of DNA Duplexes. *Angew. Chem., Int. Ed.* **2015**, *54* (4), 1144−1148.

(36) Carnegie, C.; Urbieta, M.; Chikkaraddy, R.; de Nijs, B.; Griffiths, J.; Deacon, W. M.; Kamp, M.; Zabala, N.; Aizpurua, J.; Baumberg, J. J. Flickering Nanometre-Scale Disorder in a Crystal Lattice Tracked by Plasmonic Flare Light Emission. *Nat. Commun.* **2020**, *11*, 682.

(37) Liu, J.; Cai, Z. Y.; Sun, W. X.; Wang, J. Z.; Shen, X. R.; Zhan, C.; Devasenathipathy, R.; Zhou, J. Z.; Wu, D. Y.; Mao, B. W.; Tian, Z. Q. Plasmonic Hot Electron-Mediated Hydrodehalogenation Kinetics on Nanostructured Ag Electrodes. *J. Am. Chem. Soc.* **2020**, *142* (41), 17489−17498.

(38) Murphy, C. J.; Arkin, M. R.; Jenkins, Y.; Ghatlia, N. D.; Bossmann, S. H.; Turro, N. J.; Barton, J. K. Long-Range Photo-induced Electron Transfer through a DNA Helix. *Science* **1993**, *262* (5136), 1025−1029.

(39) Arkin, M. R.; Stemp, E. D. A.; Holmlin, R. E.; Barton, J. K.; Hörmann, A.; Olson, E. J. C.; Barbara, P. F. Rates of DNA-Mediated Electron Transfer between Metallointercalators. *Science* **1996**, *273* (5274), 475−480.

(40) Kelley, S. O.; Barton, J. K.; Jackson, N. M.; Hill, M. G. Electrochemistry of Methylene Blue Bound to a DNA-Modified Electrode. *Bioconjugate Chem.* **1997**, *8* (1), 31−37.

(41) Drummond, T. G.; Hill, M. G.; Barton, J. K. Electrochemical DNA Sensors. *Nat. Biotechnol.* **2003**, *21* (10), 1192−1199.

(42) Slinker, J. D.; Muren, N. B.; Renfrew, S. E.; Barton, J. K. DNA Charge Transport over 34 nm. *Nat. Chem.* **2011**, *3* (3), 228−233.

(43) Dauphin-Ducharme, P.; Arroyo-Currás, N.; Plaxco, K. W. High-Precision Electrochemical Measurements of the Guanine-, Mismatch-, and Length-Dependence of Electron Transfer from Electrode-Bound DNA Are Consistent with a Contact-Mediated Mechanism. *J. Am. Chem. Soc.* **2019**, *141* (3), 1304−1311.

(44) Zhuravel, R.; Huang, H.; Polycarpou, G.; Polydorides, S.; Motamarri, P.; Katrivas, L.; Rotem, D.; Sperling, J.; Zotti, L. A.; Kotlyar, A. B.; Cuevas, J. C.; Gavini, V.; Skourtis, S. S.; Porath, D. Backbone Charge Transport in Double-Stranded DNA. *Nat. Nanotechnol.* **2020**, *15* (10), 836−840.

(45) Wirth, J.; Garwe, F.; Meyer, R.; Csáki, A.; Stranik, O.; Fritzsche, W. Plasmonically Enhanced Electron Escape from Gold Nanoparticles and Their Polarization-Dependent Excitation Transfer along DNA Nanowires. *Nano Lett.* **2014**, *14* (7), 3809−3816.

(46) Toppari, J. J.; Wirth, J.; Garwe, F.; Stranik, O.; Csaki, A.; Bergmann, J.; Paa, W.; Fritzsche, W. Plasmonic Coupling and Long-Range Transfer of an Excitation along a DNA Nanowire. *ACS Nano* **2013**, *7* (2), 1291−1298.

(47) Yin, X.; Wierzbinski, E.; Lu, H.; Bezer, S.; De Leon, A. R.; Davis, K. L.; Achim, C.; Waldeck, D. H. A Three-Step Kinetic Model for Electrochemical Charge Transfer in the Hopping Regime. *J. Phys. Chem. A* **2014**, *118* (35), 7579−7589.

(48) Zwang, T. J.; Tse, E. C. M.; Barton, J. K. Sensing DNA through DNA Charge Transport. *ACS Chem. Biol.* **2018**, *13*, 1799−1809.

(49) Genereux, J. C.; Barton, J. K. Mechanisms for DNA Charge Transport. *Chem. Rev.* **2010**, *110* (3), 1642−1662.

(50) Kékedy-Nagy, L.; Ferapontova, E. E. Directional Preference of DNA-Mediated Electron Transfer in Gold-Tethered DNA Duplexes: Is DNA a Molecular Rectifier? *Angew. Chem., Int. Ed.* **2019**, *58* (10), 3048−3052.

(51) Giese, B. Long-Distance Charge Transport in DNA: The Hopping Mechanism. *Acc. Chem. Res.* **2000**, *33* (9), 631−636.

(52) Drummond, T. G.; Hill, M. G.; Barton, J. K. Electron Transfer Rates in DNA Films as a Function of Tether Length. *J. Am. Chem. Soc.* **2004**, *126* (46), 15010−15011.

(53) Genereux, J. C.; Barton, J. K. Mechanisms for DNA Charge Transport. *Chem. Rev.* **2010**, *110* (3), 1642−1662.

(54) Beratan, D. N. Why are DNA and Protein Electron Transfer so Different? *Annu. Rev. Phys. Chem.* **2019**, *70* (1), 71−97.

(55) Giese, B.; Amaudrut, J.; Köhler, A. K.; Spormann, M.; Wessely, S. Direct Observation of Hole Transfer through DNA by Hopping between Adenine Bases and by Tunnelling. *Nature* **2001**, *412*, 318−320.

(56) Xiang, L.; Palma, J. L.; Bruot, C.; Mujica, V.; Ratner, M. A.; Tao, N. Intermediate Tunnelling-Hopping Regime in DNA Charge Transport. *Nat. Chem.* **2015**, *7* (3), 221−226.

(57) Li, Z.; Han, K. Long-Range Stacking Effects of Nucleobases in Charge Transfer. *ChemRxiv*, August 10, 2020. DOI: 10.26434/chemrvix.12782114.v1 (accessed November 17, 2021).

(58) Saito, I.; Takayama, M.; Sugiyama, H.; Nakatani, K.; Tsuchida, A.; Yamamoto, M. Photoinduced DNA Cleavage *via* Electron Transfer: Demonstration That Guanine Residues Located 5′ to Guanine Are the Most Electron-Donating Sites. *J. Am. Chem. Soc.* **1995**, *117* (23), 6406−6407.

(59) Giese, B.; Biland, A. Recent Developments of Charge Injection and Charge Transfer in DNA. *Chem. Commun.* **2002**, *2* (7), 667−672.

(60) Kim, Y.; Dumett Torres, D.; Jain, P. K. Activation Energies of Plasmonic Catalysts. *Nano Lett.* **2016**, *16* (5), 3399−3407.

(61) Baffou, G.; Quidant, R.; García De Abajo, F. J. Nanoscale Control of Optical Heating in Complex Plasmonic Systems. *ACS Nano* **2010**, *4*, 709−716.

(62) Baffou, G.; Quidant, R. Thermo-Plasmonics: Using Metallic Nanostructures as Nano-Sources of Heat. *Laser Photonics Rev.* **2013**, *7* (2), 171−187.

(63) Liu, B.; Liu, J. Methods for Preparing DNA-Functionalized Gold Nanoparticles, a Key Reagent of Bioanalytical Chemistry. *Anal. Methods* **2017**, *9*, 2633−2643.